Winds of Stars and Exoplanets
Proceedings IAU Symposium No. 370, 2023
A. A. Vidotto, L. Fossati & J. S. Vink, eds.
doi:10.1017/S1743921322004550

Hydrodynamic disk solutions for Be stars using HDUST

C. Arcos[1], M. Curé[1], I. Araya[2], A. Rubio[3] and A. Carciofi[3]

[1]Instituto de Física y Astronomía, Universidad de Valparaíso, Chile

[2]Vicerrectoría de Investigación, Universidad Mayor, Chile

[3]Instituto de astronomia, geofísica e ciências atmosféricas, Universidade de São Paulo, Brazil

Abstract. In this work, we implemented a hydrodynamical solution for fast rotating stars, which leaves high values of mass-loss rates and low terminal velocities of the wind. This 1D density distribution adopts a viscosity mimicking parameter which simulates a quasi-Keplerian motion. Then, it is converted to a volumetric density considering vertical hydrostatic equilibrium using a power-law scale height, as usual in viscous decretion disk models. We calculate the theoretical hydrogen emission lines and the spectral energy distribution utilizing the radiative transfer code `HDUST`. Our disk-wind structures are in agreement with viscous decretions disk models.

Keywords. stars: emission-line, Be, stars: winds, outflows, hydrodynamics

1. Introduction

Classical Be stars (CBes) are defined as fast rotating (Zorec et al. 2016; Solar et al. 2022) main sequence stars that form an equatorial gas disk rotating in a quasi-Keplerian motion (Rivinius et al. 2013). These disks are built from mass ejected from the stellar surface that acquires sufficient velocity and angular momentum to orbit the star and are referred to as decretion disks. Once ejected from the star, material in a CBe disk is generally governed by gravity and viscous forces. The Viscous Decretion Disk (VDD) model (Lee et al. 1991; Bjorkman & Wood 1997; Okazaki 2001; Bjorkman & Carciofi 2005) is currently the best theoretical framework describing the evolution of these disks once formed. Viscosity acts to shuffle the angular momentum of the circumstellar material. A small fraction (∼1%) of the mass ejected by the star acquires sufficient angular momentum to move outwards, orbiting at increasing radii. In contrast, most of the ejected mass falls back onto the star (Haubois et al. 2012). The strength of viscosity is parameterized as in the model from Shakura (1973) and dictates the timescales over which Be star decretion disks evolve and dissipate.

The disk feeding process is still not well understood. It is probably a combination of some mechanisms such as non-radial pulsation, stellar winds, and fast rotation, since these features are usually observed in these stars. Recent works (Kee et al. 2018b,a) indicate that, in addition to viscosity, radiative ablation may play a role in the mass budget of CBe disks by systematically removing (employing radiative acceleration) some material from the inner part of CBe disks, thus forming a disk-wind type of structure both above and below the disk.

Under the hypothesis that these structures are fed like radiation-driven winds and the rotation of the central star plays an important role in shaping the disk, in this work, we study the interplay of a particular hydrodynamic solution called Ω-slow (Curé 2004; Araya et al. 2017) to test a physical model for Be stars outflows.

2. VDD parametric model

The parametric model for the volumetric density distribution depends on the radial distance from the star, r, and the height above the equatorial plane, z, and has the form

$$\rho(r,z) = \rho_0 \left(\frac{r}{R_\star}\right)^{-m} \exp\left(\frac{-z^2}{2H^2}\right), \tag{2.1}$$

where ρ_0 is the disk base density, $R_\star$ is the stellar radius and H is the height scale given by

$$H = H_0 \left(\frac{r}{R_\star}\right)^{\beta}. \tag{2.2}$$

For isothermal disks β=3/2 and the constant H_0 is defined by

$$H_0 = \left(\frac{2R_\star^3 kT_0}{GM_\star \mu_0 m_H}\right)^{1/2}, \tag{2.3}$$

where $M_\star$ is the stellar mass, G is the gravitational constant, m_H is the mass of a hydrogen atom, k is the Boltzmann constant, μ_0 is the mean molecular weight of the gas and T_0 is an isothermal temperature used only to fix the vertical structure of the disk initially. In this work we set μ_0=0.6 and T_0=0.72 $T_{\rm eff}$. This steady-state and isothermal power-law approximation has been extensively used in the literature, achieving good agreement with observations (Carciofi & Bjorkman 2006; Carciofi et al. 2009; Jones et al. 2008; Klement et al. 2015; Silaj et al. 2016; Arcos et al. 2017).

3. Ω-slow solution for Be stars

Curé (2004) found a new hydrodynamical solution from the standard radiation-driven winds theory (Castor et al. 1975; Friend & Abbott 1986). This is called Ω-slow solution and appears for fast rotating stars, $\Omega = v_{rot}/v_{crit} \gtrsim 0.75$. This solution is characterized by a slow wind with high values of mass-loss rates. However, it assumes angular momentum conservation and its terminal velocity is too fast to explain the Be disks. Currently, the disk-like structure observed in Be stars is modeled using a quasi-Keplerian motion.

Okazaki (2001) used viscosity and the model of a radiative force due to an ensemble of optically-thin lines from Chen & Marlborough (1994). In their model, the radiation force is always an increasing function of the radial coordinate and does not decay at large distances as it should happen. Therefore, based on the results of the Ω-slow solution, we implemented a radiative force that increases near the stellar surface and after particular distance decay in terms of the radial coordinate. We followed the procedure made by de Araujo (1995) implementing a mimicking viscosity parameter via

$$V_\phi = \Omega \sqrt{\frac{GM_\star(1-\Gamma)}{R_\star}} \left(\frac{R_\star}{r}\right)^{\gamma_{vis}}, \tag{3.1}$$

where V_ϕ is the rotational velocity component of the wind in the equatorial plane, Γ considers the mean opacity of the total flux and γ_{vis} is the viscosity mimicking parameter. For $\gamma_{vis} = 0.5$ a Keplerian outflowing wind is obtained.

In Figure 1 we compare two wind density distributions (dotted blue and dot-dashed red lines) obtained under our procedure described above. Both solutions were generated considering a high rotational speed with Ω=0.99 and fixing the line-force parameters δ=0 and k=0.2 for a γ_{vis}=0.51 (quasi-Keplerian motion). The stellar parameters are for a B2V star, with $T_{\rm eff}$=21000 K, log g = 4.00 and $R_\star$=4.5 $R_\odot$. We set the base density to ρ_0=5×10^{-11} g/cm^3 which is a typical value for a B2Ve star (see Arcos et al. 2017; Vieira et al. 2017). The wind parameters obtained by these models are summarized in

https://doi.org/10.1017/S1743921322004550 Published online by Cambridge University Press

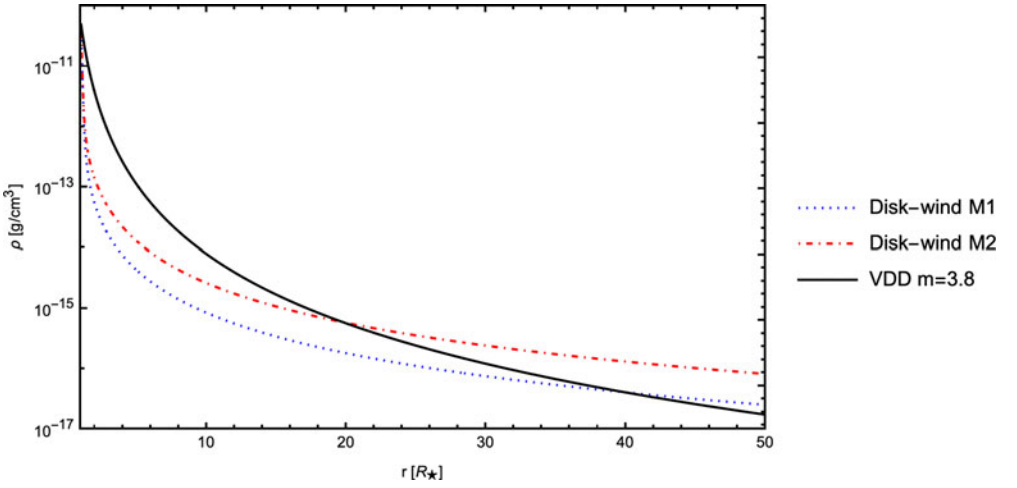

Figure 1. Equatorial density distributions for the models used in this work. Line force parameters for the wind are displayed in Table 1. Both hydrodynamical solutions are compared to a VDD model with an exponent power-law m=3.8 represented by the solid black line.

Table 1. Wind density description. Models were generated with δ=0, Ω=0.99 and a base density ρ_0=5×10^{-11} g/cm^3. The stellar parameters are those for a typical B2V star, with $T_{\rm eff}$=21000 K, log g = 4.00 and $R_\star$=4.5 $R_\odot$.

Model	α	k	γ_{vis}	$\dot{M}$ (10^{-8} $M_\odot$/yr)	v_∞ (km/s)
M1	0.50	0.2	0.51	1.17	101
M2	0.62	0.2	0.51	4.98	131

Table 1 where a denser, slower solution is observed compared to a standard fast solution. The best representation of the equatorial density structure from our hydrodynamical models is for a VDD parametric model with exponent m=3.8 (solid black line overplotted in Fig. 1). The figure shows that the density of the hydrodynamical solutions decay much faster near the stellar photosphere ($\sim$ one order of magnitude at 5 $R_\star$) than the standard VDD model. This would imply less flux contribution (emission-line intensity) to the emitting region enclosed by Hα, usually considered as the size of the disk in the optical range. In addition, both hydrodynamical solutions overpass the VDD model at some point, e.g., model M1 does it at $\sim$20 $R_\star$ and M2 at $\sim$40 $R_\star$, then for pole-on views we will expect that the emission-lines will be more intense than the ones obtained with VDD models.

4. Disk-wind structure

To perform the radiative transfer calculations using our hydrodynamical wind solutions, we used of the 3D Monte Carlo radiative transfer code, `HDUST` (Carciofi & Bjorkman 2006, 2008). The code computes the spectral energy distribution (SED), polarization and Hydrogen lines for different lines of sight. In addition, it allows several input options for the density distribution and motion of the disk. Also, it considers the oblateness of the rotating star and, thus, the gravity darkening effects.

Our first step was creating a conversion code to appropriately situate our 1D hydrodynamical solutions to be read by `HDUST`. The adopted grid structure is divided in 50 radial cells (N_r), 42 co-latitudinal cells (N_μ) and 1 azimuthal cells (N_ϕ, axisymmetry). Thus, the 1D density input is distributed into a 3D geometry in the equatorial plane by setting vertical hydrostatic equilibrium with a power-law height scale (see eq. 2.2).

https://doi.org/10.1017/S1743921322004550 Published online by Cambridge University Press

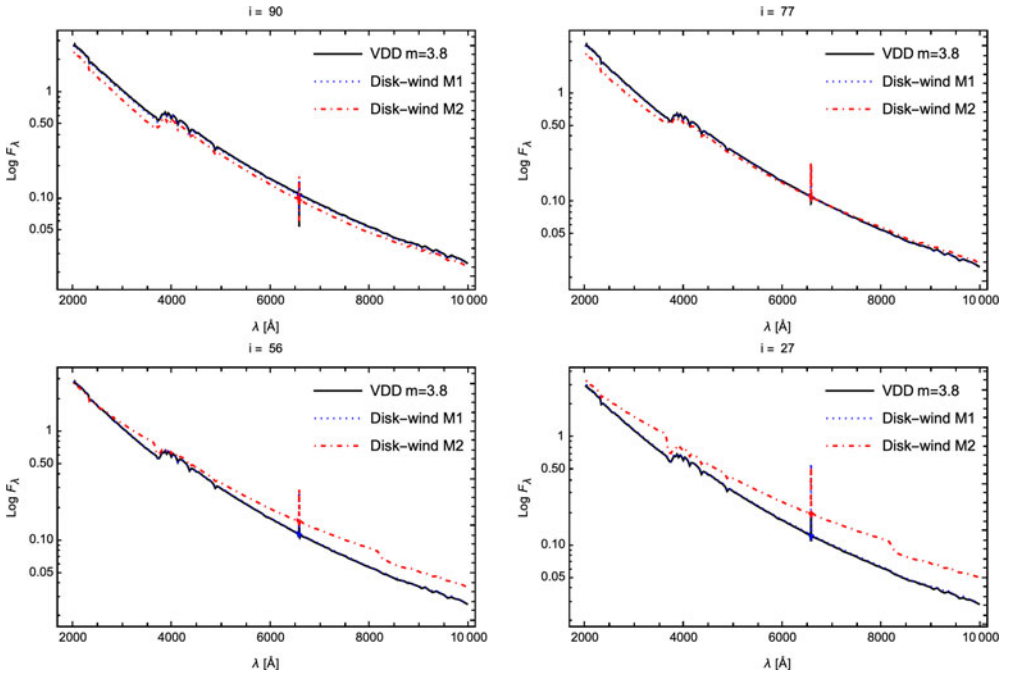

Figure 2. SED computed by HDUST code for the disk-wind and VDD models.

The second step was to use this hydrodynamical density distribution for the wind as input in the HDUST code. We set a disk size of 50 $R_\star$ and a parametric rigid rotator star without oblateness (because our hydrodynamical solution was created with a spherical geometry). The stellar spectrum was defined by a Kurucz (1994) model and the limb darkening from Claret (2000) models. We calculated the SED and the theoretical Hα emission line with this setup. Fig. 2 shows the SED for our wind models computed with HDUST. We present the result for four different inclination angles, starting at edge-on view (i=90°) up to pole-on view (i=27°). The output flux is dimensionless (we are using it only for comparison proposes) and is in logarithm scale to appreciate the differences. The VDD model from Fig. 1 is over-plotted to our wind solutions and is represented with a solid black line. From the figure, we can see that the shape of the density distribution affects directly the flux continuum, having the VDD and model M1 similar slopes (but different fluxes, see Fig. 1) compared to the M2 model which is denser and thus, more optically thick, absorbing more photons at the edge-on view.

In the case of the Hα emission line, the results are displayed in Fig. 3 for the two wind models and the VDD comparison. The sub-figures at the top have a different vertical scale than those at the bottom. At the equatorial view, the VDD model (solid black line) has the highest intensity, as we expected from the density distribution (Fig. 1). Because the density from the model M2 decays faster than the VDD, but from $\sim$20 $R_\star$, it compensates by increasing its intensity, then a similar line-emission is observed but with a different shape. We note models have different densities, but same velocities, therefore since the slower components of the Hα line come from a denser region, they are more intense. The opposite behavior is observed close to the pole when the wind model is almost twice in intensity compared with VDD (see Fig. 3 at i=27°). From the disk temperature distribution, all models show similar behavior to a 'U' shape profile, as shown in Carciofi & Bjorkman (2006), but with different locations for the minimum temperature in the disk, being closer to the star with high slopes of density decay. Model

https://doi.org/10.1017/S1743921322004550 Published online by Cambridge University Press

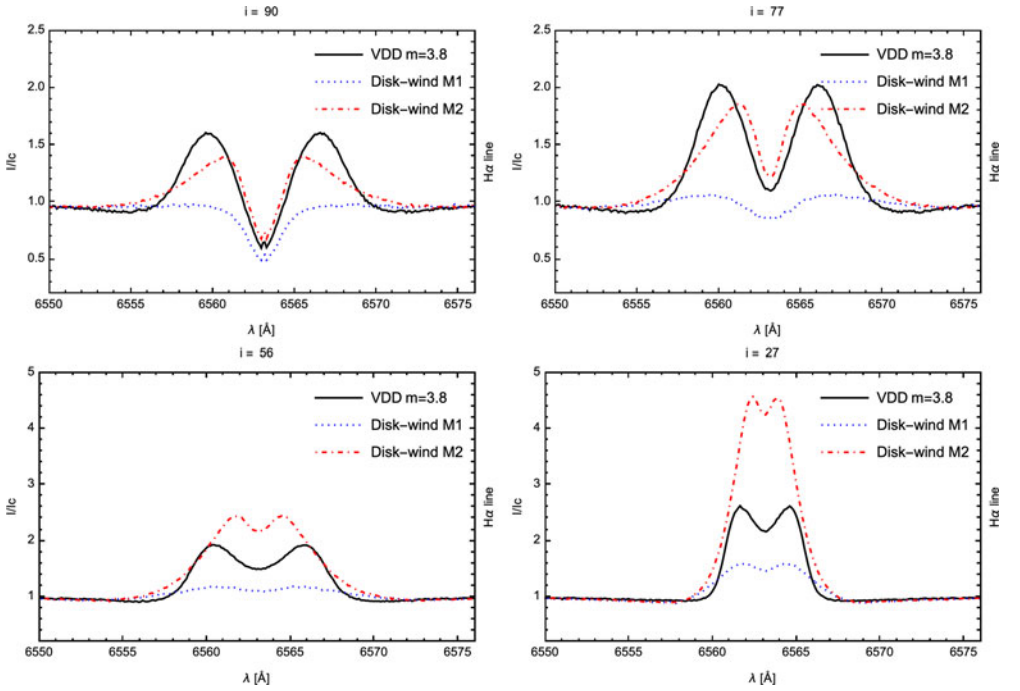

Figure 3. Hα theoretical emission line computed with HDUST for the different wind models and the VDD comparison. The sub-figures at the top have a different vertical scale than those at the bottom. This theoretical line profiles were generated with the density distributions shown in Fig. 1.

M1 (dotted blue line) does not have enough density to form a suitable emission line (as we expected with the other models). Therefore, these density distributions better describe dissipating or forming disk phases. We note that the emission line generated with this solution is all the time under the VDD model, as we expected from Fig. 1.

5. Summary and discussion

Massive stars possess strong stellar winds driven by radiation, usually with high mass-loss rates and terminal velocities. CBes are massive stars on the main sequence, which enhance the mass-loss rates at the stellar equator, forming and dissipating a quasi-keplerian rotating gas disk under some unknown process. In order to understand the physical process these stars go through, we test the Ω-slow hydrodynamical solution for stars rotating faster than 75% of their critical rotation. This solution leads to high values of mass-loss rates and slow terminal velocities. In addition, we adopt a viscosity parameter for the azimuthal velocity to reach a quasi-Keplerian gas motion. By using the radiative transport code HDUST and forcing vertical hydrostatic equilibrium, our preliminary results successfully reproduce a similar theoretical line-emission shape for a typical B2Ve star. These preliminary results were made under a spherical symmetry; thus, gravity darkening effects are not considered here. Also, we note that our density distribution decays too fast near the stellar surface, with differences close to one order of magnitude compared to the VDD model; as a result, a low intensity in the Hα emission line. More tests must be done, with different values of Ω covering other spectral types. Once having several models with disk-wind structures, the next step is to compare with spectroscopic and photometric observations of several Be stars.

https://doi.org/10.1017/S1743921322004550 Published online by Cambridge University Press

Acknowledgments

Authors thank project ANID-FAPESP N°133541. CA and IA thanks FONDECYT 11190945 and 11190147, respectively. MC, CA & IA are grateful to projects FONDECYT 1190485. This work has been possible thanks to the use of AWS-UChile-NLHPC credits. Powered@NLHPC: This research was partially supported by the super-computing infrastructure of the NLHPC (ECM-02). This project has also received funding from the European Union's Framework Programme for Research and Innovation Horizon 2020 (2014–2020) under the Marie Skłodowska-Curie grant Agreement No 823734. ACC acknowledges support from CNPq (grant 311446/2019-1) and FAPESP (grants 2018/04055-8 and 2019/13354-1). ACR acknowledges support from CAPES (grant 88887.464563/2019-00) and DAAD (reference number 91819449).

References

Araya, I., Jones, C. E., Curé, M., et al. 2017, ApJ, 846, 2
Arcos, C., Jones, C. E., Sigut, T. A. A., Kanaan, S., & Curé, M. 2017, ApJ, 842, 48
Bjorkman, J. E. & Carciofi, A. C. 2005, in Astronomical Society of the Pacific Conference Series, Vol. 343, Astronomical Polarimetry: Current Status and Future Directions, ed. A. Adamson, C. Aspin, C. Davis, & T. Fujiyoshi, 270
Bjorkman, J. E. & Wood, K. 1997, in American Astronomical Society Meeting Abstracts, Vol. 191, American Astronomical Society Meeting Abstracts, 12.04
Carciofi, A. C. & Bjorkman, J. E. 2006, ApJ, 639, 1081
Carciofi, A. C. & Bjorkman, J. E. 2008, ApJ, 684, 1374
Carciofi, A. C., Okazaki, A. T., Le Bouquin, J. B., et al. 2009, A&A, 504, 915
Castor, J. I., Abbott, D. C., & Klein, R. I. 1975, ApJ, 195, 157
Chen, H. & Marlborough, J. M. 1994, ApJ, 427, 1005
Claret, A. 2000, A&A, 363, 1081
Curé, M. 2004, ApJ, 614, 929
de Araujo, F. X. 1995, A&A, 298, 179
Friend, D. B. & Abbott, D. C. 1986, ApJ, 311, 701
Haubois, X., Carciofi, A. C., Rivinius, T., Okazaki, A. T., & Bjorkman, J. E. 2012, ApJ, 756, 156
Jones, C. E., Tycner, C., Sigut, T. A. A., Benson, J. A., & Hutter, D. J. 2008, ApJ, 687, 598
Kee, N. D., Owocki, S., & Kuiper, R. 2018a, MNRAS, 474, 847
Kee, N. D., Owocki, S., & Kuiper, R. 2018b, MNRAS, 479, 4633
Klement, R., Carciofi, A. C., Rivinius, T., et al. 2015, A&A, 584, A85
Kurucz, R. 1994, Solar abundance model atmospheres for 0, 19
Lee, U., Osaki, Y., & Saio, H. 1991, MNRAS, 250, 432
Okazaki, A. T. 2001, PASJ, 53, 119
Rivinius, T., Carciofi, A. C., & Martayan, C. 2013, AAPR, 21, 69
Shakura, N. I. 1973, SOVAST, 16, 756
Silaj, J., Jones, C. E., Carciofi, A. C., et al. 2016, ApJ, 826, 81
Solar, M., Arcos, C., Curé, M., Levenhagen, R. S., & Araya, I. 2022, MNRAS, 511, 4404
Vieira, R. G., Carciofi, A. C., Bjorkman, J. E., et al. 2017, MNRAS, 464, 3071
Zorec, J., Frémat, Y., Domiciano de Souza, A., et al. 2016, A&A, 595, A132